Height prediction in Directed Metal Deposition with Artificial Neural Networks

Available online at www.sciencedirect.com

ScienceDirect

Procedia CIRP 113 (2022) 312–317

www.elsevier.com/locate/procedia

ISEM XXI

Height prediction in Directed Metal Deposition with Artificial Neural Networks

Daniel Knüttel[a,b*], Stefano Baraldo[c], Anna Valente[c], Emanuele Carpanzano[c], Konrad Wegener[b]

[a]*Intelligent Production Machines, Inspire AG, Via la Santa 1, Viganello 6962, Switzerland*
[b]*ETH Zürich, IWF - Institute for Machine Tools and Manufacturing, Leonhardstrasse 21, Zurich 8092, Switzerland*
[c]*SUPSI, Department of Innovative Technologies, Via la Santa 1, Viganello 6962, Switzerland*

* Corresponding author. Tel.: +41 58 666 67 08; *E-mail address:* knuettel@iwf.mavt.ethz.ch

Abstract

Directed Metal Deposition (DMD) is a promising metal additive manufacturing technology, where parts are manufactured by fusing injected metal powder particles with a laser beam moving along a predefined trajectory. A toolpath typically includes sections as curves or edges, where machine axes need to decelerate and accelerate accordingly. As a result, the locally applied laser energy and powder density vary during the deposition process, leading to local over-deposition and over-heating. These deviations are additionally influenced by the toolpath geometry and process duration: previous depositions can influence close toolpath segments, in terms of time and space, resulting in local heat accumulations and develop profiles and microstructures that are different from the ones generated in other segments deposited with the same parameters due to geometry- and temperature dependent catchment profiles. To prevent these phenomena, lightweight and scalable models are required to predict the process behaviour for variable toolpaths.
In this work, an artificial intelligence-based approach is presented to handle the process complexity and the multitude of toolpath variations for Inconel 718. Artificial neural networks (ANN) are used to predict the height of the deposition considering the previously defined toolpath. Training data have been generated by printing a randomized toolpath containing multiple curvatures and geometries. Based on the trained models, significant local geometric deviations are successfully predicted for the complete toolpath and could be anticipated by adapting process parameters accordingly.

Keywords: Neural network, Directed Metal Deposition, Deposition height

1. Introduction

Additive manufacturing (AM) processes enable the production and repairing of components with complex geometries, leading to lightweight parts with highly customized shapes and properties [1]. Typical applications are in the aeronautic, oil&gas or prosthetics industry, where specialized components made of high-performance alloys as Inconel 718 are needed to meet the requirements of elevated operating temperature, mechanical and chemical requirements. In particular, Direct Metal Deposition (DMD) is a promising manufacturing process to efficiently repair high value parts or to build complex work pieces from scratch [2]. Despite its multiple benefits, the complexity of the involved phenomena (powder-gas dynamics, phase changes, thermo-mechanical coupling, parameter uncertainty) make this process hard to master, and the definition of optimal process recipes and strategies often requires intensive trial-and-error to avoid dimensional deviations and meet material integrity requirements [3]. To overcome these issues, the approaches

2212-8271
10.1016/j.procir.2022.09.108

adopted by researchers range from multi-physics simulations to in-process monitoring and control.

Recent progress in the field of multi-physics simulation achieved meaningful results and revealed important insights into the process behavior. Wirth et al. [4] presented a multi-physics simulation approach, able to predict accurately the temperature distribution and height of single tracks. However, the high process dynamics and various physical phenomena lead to complex models limiting the effectiveness of multi-physics-based process prediction. The high computational complexity of such models makes simulation of a full part impractical even for small-sized components and therefore unsuitable for control applications [5].

On the other side, the harsh process environment and dynamics limit the integration and efficiency of monitoring systems [6]. For example, Baraldo et al. [7] presented a promising closed loop approach to reduce over-depositions by modulating the laser power: the mean image intensity of real-time melt pool images is correlated with the deposition height, thus allowing to locally adapt the laser power and to reduce the over-deposition rate. Another approach has been proposed by Hua et al. [8], who implemented an inline height measurement system to control the deposition height in real-time. A further, model-based approach to on-line control has been presented by Wang et al. [9], using a previously developed lumped model [10] for the implementation of a nonlinear inverse-dynamics controller to regulate the build height.

However, basing parameter modulation purely on process feedbacks is often insufficient to optimize the deposition process. Defects due to very fast dynamics (e.g. laser steps, sudden acceleration) cannot be corrected timely by just waiting to observe them; therefore, feed-forward process modelling and control are essential, but they should rely on lean approaches to be exploitable in real applications. In this view, Caiazzo et al. [11] performed offline prediction of deposition height via machine learning (ML): they trained a neural network (NN) that predicts the average deposition height of a single, straight track based on the process parameters, to determine the most suitable recipe before starting the manufacturing process. However, this approach is limited to single and straight tracks. Moving to a local scale, Woo et al. [12] investigated experimentally the effects of geometric deviations in corners and subsequently applied a scanning speed control algorithm to achieve uniform height over the corners.

The present work extends the state of the art of ML-based DMD process prediction by additionally predicting the local deposition height over the whole trajectory. The prediction process could be performed off-line before starting the manufacturing process to anticipate over-depositions, thus enabling an effective feed-forward control solution. Combining this approach with existing inline process controls could even further improve the system performance.

The presented approach is developed with a focus on complex toolpaths characterized by multiple changes of direction. The methodology and experimental set-up for the data generation are described in Section 2. Based on the training data neural networks are optimized and the obtained results are presented and discussed in Section 3, while Section 4 outlines the key findings and next steps to further improve the approach and its application.

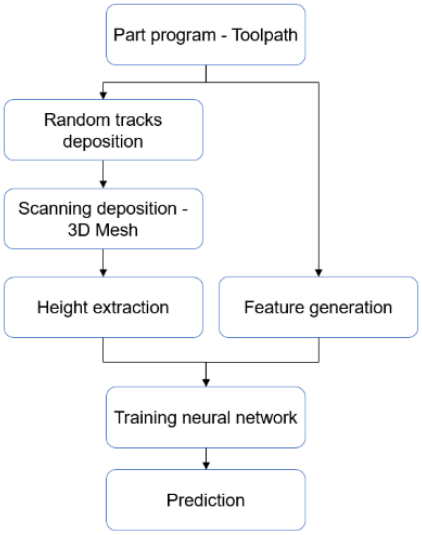

Fig. 1. Process flow of the DMD height prediction.

2. Methodology

The high-level approach consists in the following steps described in Fig. 1. First of all, the experimental campaign is designed, by generating the tool paths and the corresponding part program. To obtain process outcomes, i.e. deposition height, the deposition is performed, and the resulting geometries are acquired off-line with a laser scanning confocal microscope; the obtained 3D mesh is then processed to extract the height of the deposited track along the tool path. On the other side, trajectory and process input parameters are translated into features that are potentially relevant to predict the deposition height (see Section 2.1 and 2.2). Finally, the designed NN model is trained, using the previously defined features as inputs, to predict the height profile of the generated tool path. Key steps of the pipeline are detailed in the following.

2.1. Experimental set-up

Experimental data are generated by building test samples composed by tracks with random corners (*random tracks*), as shown in Fig. 2. The substrate and the powder consist of Inconel 718 nickel alloy. The tracks are produced with a Prima Power Laserdyne 430 3-axis CNC machine with a four-nozzle

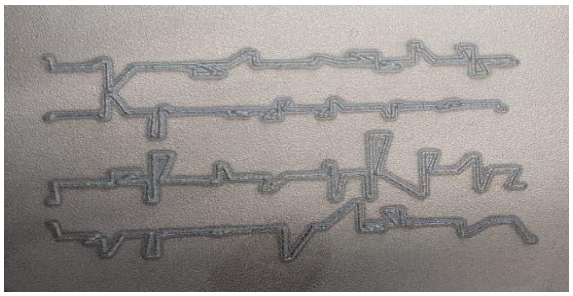

Fig. 2. Deposited random track with a total length of 65 mm.

Optomec DMD head. In all the experiments, the laser power is set to 300 W with a scanning speed of 600 mm/min. Table 1 summarizes the applied process parameters.

Table 1. Process parameters

Parameter	Value
Laser power	300 W
Scan speed	600 mm/min
Powder feed	0.099 g/s
Nozzles	4
Material	Inconel 718
Powder size	45 – 106 µm
Argon carrier gas	4 l/min
Argon shielding gas	15 l/min

Four consecutive tracks are deposited on each substrate. Each track is generated randomly by concatenating random consecutive sections of variable length and angles, with the scope of covering various angles and local curvatures, leading to enhanced geometrical deviations due to the local over-deposition. During the process, the actual toolpath including its X and Y coordinates is logged at 1 kHz, to allow an accurate reconstruction of process dynamics.

An integrated dataset, where the laser spot position and resulting track height are synchronized, is required to train the proposed NN model. To achieve this, the tracks are scanned off-line with a Keyence VK-X1000, a 3D laser scanning confocal microscope, to generate a triangulated mesh of the sample. Afterwards, the mesh is processed with a custom MATLAB script to extract the track height at each tool path sampling point, as described in [13].

2.2. Feature generation

Based on the toolpath of the random track, various features, i.e. derived process variables, are determined, with the scope to cover important characteristics that establish relevant relationships between the trajectory and the actual deposition height. The most intuitive features are for example velocity and acceleration for each time step of the trajectory. Thereby the velocity is determined by the machine logged coordinates during the process and the according timestep. In particular, local velocity reaching zero indicates the presence of a corner and correlates strongly with the local energy density; for example, with faster scanning speed and constant laser power, the local energy density and the resulting deposition height decrease significantly.

Two additional features account for increases of energy density due to the deposition geometry: angle and curvatures. The angle feature corresponds to the angle width of the corner that is nearest to the considered point. The curvature features instead are determined by the following procedure: sliding time windows of 1 ms, 5 ms, 10 ms, 50 ms, 100 ms and 200 ms are moved along the toolpath; two vectors are defined at each time instant, connecting the trajectory point at the center of the time window with the points defined by the starting/ending times of the window itself. Finally, the angle between the two vectors is determined. An example of the resulting curvatures is shown in Fig. 3. Introducing simultaneously curvatures computed on

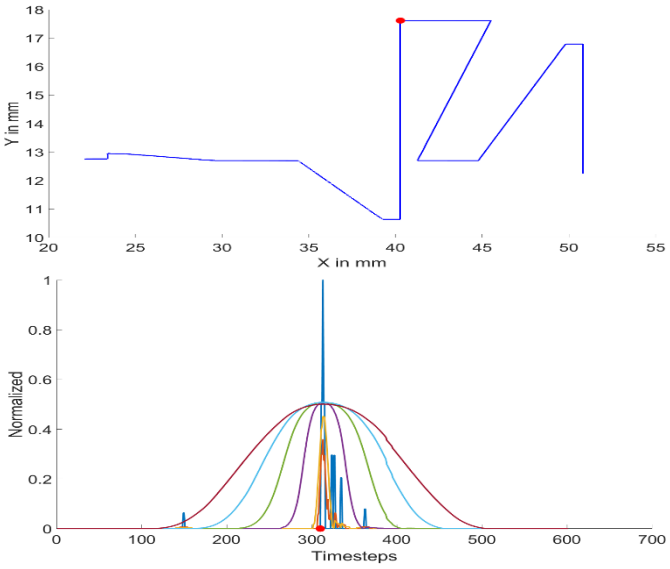

Fig. 3. The upper plot illustrates a section of the toolpath, where the red dot indicates the location of the curvature features at timestep 300 in the lower plot.

multiple scales allows to capture in advance the approach to a corner (large time windows), without losing the detail of the sudden change of direction (small time windows)

A further potentially influencing factor is the proximity of depositions to previously deposited track segments. During a deposition, local heating occurs in the substrate region that surrounds the laser spot. Therefore, substrate pre-heating potentially increases the deposition height of successive depositions in that area, leading to local height deviations [14]. To account for this effect, a proximity feature has been defined by counting the amount of tool path points in a predefined neighborhood of the considered position. The proximity index considers only trajectory elements visited previously to the current position. In case of elements close to previous depositions, the index will be higher and thus relevant in the prediction.

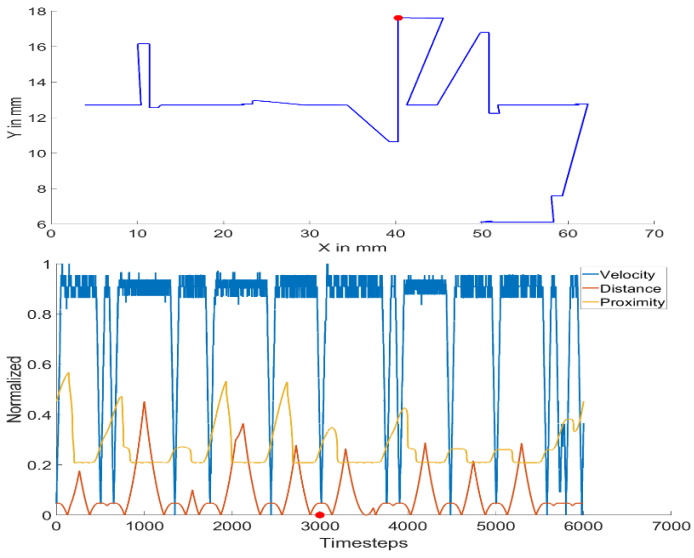

Fig. 4. The upper plot illustrates a section of the toolpath, where the red dot indicates the location of the distance and proximity features in the lower plot. The corresponding location in the lower plot is indicated by the red rot.

Another feature is introduced to describe the *distance* of the current position from the nearest corner. Depending on the distance, the heat accumulation due to curvature varies and impacts differently the deposition height. Based on such distance, a further feature is generated by weighting the distance with the angle of the nearest corner. Fig. 4. shows an exemplary section of the random track and the distance feature. Furthermore, the proximity and velocity are displayed in the graph. The minima of the velocity indicate the location of the corners. The final dataset contains the features summarized in Table 2.

Table 2. Features of the dataset

Parameter	Value ranges
Velocity	[0, 0.011] mm/s
Acceleration	[0, 0.00024] mm/s2
Angle	[2.9, 178] °
Curvatures for 1 ms, 5 ms, 50 ms, 100 ms, 150 ms, 200 ms,	e.g. for 200 ms [0, 3.139]
Proximity	[1, 959]
Distance	[0, 20.89] mm
Distance weighted by the angle	[0, 4.29] mm/°

Before training the NN, the dataset composed by the aforementioned features is normalized to a range between 0 and 1, to stabilize and accelerate the training process.

2.3. Neural network

Neural networks (NN) are exploited to predict the deposition height based on the previously defined features. The architecture used for the NN is a fully connected network, consisting of multiple sequential layers. An exemplary architecture is shown in Fig. 5. In general, the relation between the vector of inputs $\boldsymbol{z}_{i-1}$ and the output $\mathbf{z}_i$ of the i^{th} layer is defined as

$$\boldsymbol{z_i} = \sigma_i(\boldsymbol{W}_i^T \boldsymbol{z_{i-1}} + \boldsymbol{b}_i), \tag{1}$$

where σ_i is the activation function, $\mathbf{W}_i^T$ is the weight matrix of the layer and $\boldsymbol{b}_i$ the bias vector. The activation function introduces the non-linearity of the system. Typical activation functions are tanh, sigmoid and the within this work used rectified linear unit (ReLU). The training of the neural network optimizes the weights to reduce the loss function. Common optimizers are based on stochastic gradient descent, such as the Adam optimizer also used in this work [15].

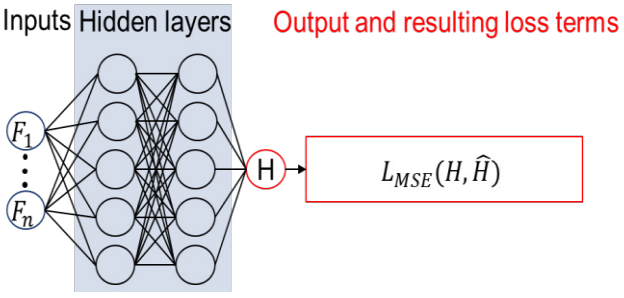

Fig. 5: Exemplary fully connected neural network with two hidden layers and a mean squared error loss function. F_1, …, F_n correspond to the feature inputs, $\hat{H}$ is the predicted height and H is the ground truth.

A crucial element in the estimation procedure is the loss function, which defines the criterion upon which the NN should try to optimize. A common loss function is the mean squared error:

$$L_{MSE}(H, \hat{H}) = \frac{1}{n} \sum_{n=1}^{n} (H_i - \hat{H}_i)^2, \tag{2}$$

which penalizes the difference between the prediction $\hat{H}_i$ and the known value H_i; the optimizer will therefore try to iteratively modify the NN weights so that this difference is kept as small as possible across all data until the training terminates with achieving the number of epochs.

3. Results & Discussion

The previously defined features are computed for each point on the toolpath and combined with the corresponding height. The dataset is divided into a training and test set, to avoid an overfitting of the trained model. In this case, tracks 1 to 3 are used for the training of the neural network and track 4 for testing purposes (see Fig. 1.). The relatively small amount of training data requires less than 1GB of memory, thus enabling the usage of a maximal batch size equal to the amount of training data. The model is set-up in Python with PyTorch and the computations are executed on a graphical processor unit (GPU) Nvidia Quadro M4000 to accelerate the training process.

3.1. Model training and optimization

At first, the feasibility of the height prediction is demonstrated by using 70 % of the previously computed features to train a neural network with 10 layers and 200 neurons, while the remaining 30 % of the dataset are used as a validation set.

The training set consist of 43’921 data points and is trained over 5’000 epochs with an initial learning rate of 0.0001. The learning rate is reduced every 500 epochs by a factor of 0.8. The training takes about 100 minutes with a maximum batch size equal to the amount of training data.

In a second step, the model is optimized by tuning main hyperparameters as the number of hidden layers, width of each layer, amount of training data and optimization parameters. In particular, a scheduler is implemented to decrease the learning rate by a pre-defined factor (gamma) after a certain number of epochs (scheduler step). This enables an improved optimization process by minimizing the loss with bigger steps during the first epochs and performing smaller weight adjustments with ongoing training progress. Table 3 summarizes the performed hyperparameter variations.

Table 3. Hyperparameter variations

Parameter	Variations
Learning rate	0.0001
Training data ratio	0.5, 0.6, 0.7, 0.8, 0,9
Epochs	500, 1'000, 2'000, 3'000, 4'000, 5'000
Layers	1, 2, 3, 5, 7, 10
Neurons/layer	10, 25, 50, 100, 150, 200, 250, 300, 350

3.2. Model performance

The prediction for the validation dataset of the first feasibility results in a root mean squared error (RMSE) of 0.068 mm. Fig. 6 visualizes the prediction and the actual height for the test set.

After optimizing the hyperparameters listed in Table 3, the best model performance is obtained with 5'000 epochs, a training data ratio of 70 %, 3 hidden layers, 25 neurons/layer, a learning rate 0.0001 with a scheduler step of 500 and gamma equal to 0.8. The resulting RMSE improves through the model optimization from 0.068 mm to 0.0526 mm.

As shown in Fig. 6, the prediction matches the actual height quite well. The most relevant deviations are found in areas with multiple, concentrated sharp corners, as shown in Fig. 7, where

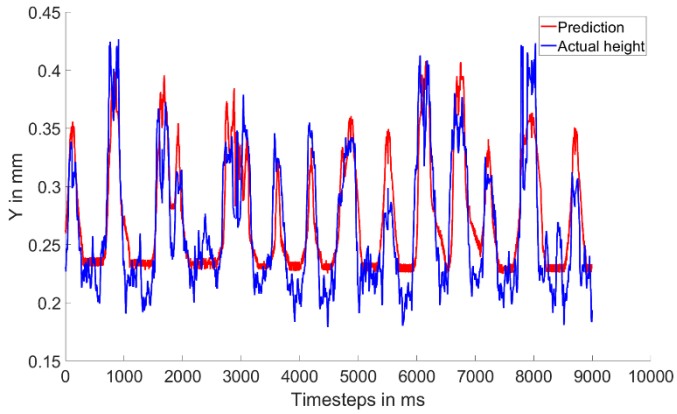

Fig. 6. Extract of the test set comparing the height prediction and actual height.

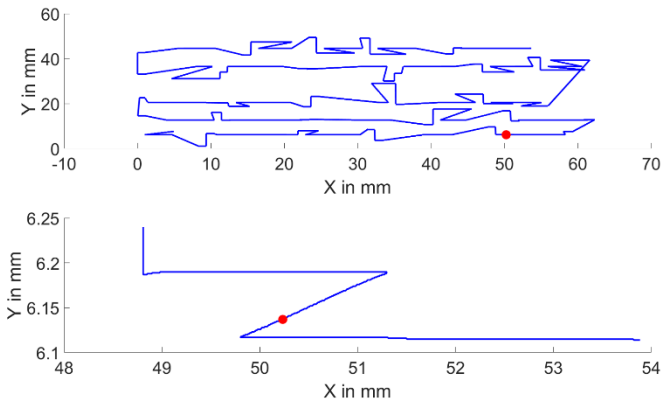

Fig. 7. The upper plot displays the toolpath and highlights the considered region zoomed in the plot below. The toolpath below shows the consecutive sharp corners leading to local "extreme" over-depositions.

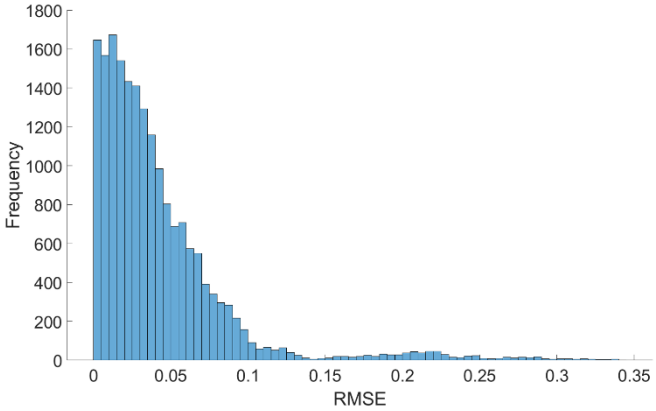

Fig. 8. Error distribution for the test set. The prediction is computed with a neural network of 5 layers, width of 200, gamma of 0.8, train ratio of 0.7 and a scheduler step of 500.

the pattern that yields a locally extreme over-deposition equal to a height of about 770 µm is shown. As a result, in similar cases the predicted height is significantly higher.

Furthermore, the process suffers from high local variances during the deposition. This can be seen in particular on straight deposition lines as shown in Fig 6. Due to this noisy behavior, many small prediction errors occur even if the prediction follows the actual height quite well. The histogram in Fig. 8 illustrates the error distribution of the RMSE. Thereby it can be clearly seen that, although few local, large errors are present, most of the model residuals are concentrated below 0.1 mm, the order of magnitude of the used powder particle size.

4. Conclusion and outlook

The presented work demonstrates the feasibility of height prediction for a complete DMD process trajectory. The results highlight the possibility to effectively predict local over-deposition through NNs. The prediction follows the behavior of the actual height in a coherent way, except in isolated regions where small deviations are due to the noisy process behavior. Furthermore, the printed random tracks contain some very sharp and consecutive corners, leading to excessive geometrical deviations. Based on the trained model, it would be possible to anticipate and minimize the over-depositions by locally adapting the laser power, thus enabling feed-forward process control. The compensation of over- and under-deposition will be part of future work. Future work will include the validation of the model for multiple parameter combinations. Thereby the process parameters will be included as additional features for the neural network. Furthermore, the influence of the substrate surface structure and material will be analyzed. Once a reliable model is established, predictive controllers could modulate the laser power to reduce over-depositions.

Acknowledgements

The research in this paper has been partially founded by SNSF project Ground Control (Grant 179014) and by EU H2020 project AMATHO (Funding Agreement ID 717194).

References

[1] A. Saboori, A. Aversa, G. Marchese, S. Biamino, M. Lombardi, P. Fino, Application of directed energy deposition-based additive manufacturing in repair, Appl. Sci. 9 (2019). https://doi.org/10.3390/app9163316.

[2] D. Svetlizky, M. Das, B. Zheng, A.L. Vyatskikh, S. Bose, A. Bandyopadhyay, J.M. Schoenung, E.J. Lavernia, N. Eliaz, Directed energy deposition (DED) additive manufacturing: Physical characteristics, defects, challenges and applications, Mater. Today. xxx (2021). https://doi.org/10.1016/j.mattod.2021.03.020.

[3] F. Mazzucato, O. Avram, A. Valente, E. Carpanzano, Recent Advances Toward the Industrialization of Metal Additive Manufacturing, Syst. Eng. Fourth Ind. Revolut. (2019) 273–319. https://doi.org/10.1002/9781119513957.ch12.

[4] F. Wirth, K. Wegener, A physical modeling and predictive simulation of the laser cladding process, Addit. Manuf. 22 (2018) 307–319. https://doi.org/10.1016/j.addma.2018.05.017.

[5] D. Knüttel, S. Baraldo, A. Valente, K. Wegener, E. Carpanzano, Model based learning for efficient modelling of heat transfer dynamics, Procedia CIRP. 102 (2021) 252–257. https://doi.org/10.1016/j.procir.2021.09.043.

[6] Z. jue Tang, W. wei Liu, Y. wen Wang, K.M. Saleheen, Z. chao Liu, S. tong Peng, Z. Zhang, H. chao Zhang, A review on in situ monitoring technology for directed energy deposition of metals, Int. J. Adv. Manuf. Technol. 108 (2020) 3437–3463. https://doi.org/10.1007/s00170-020-05569-3.

[7] S. Baraldo, A. Vandone, A. Valente, E. Carpanzano, Closed-Loop Control by Laser Power Modulation in Direct Energy Deposition Additive Manufacturing, in: L. Wang, V.D. Majstorovic, D. Mourtzis, E. Carpanzano, G. Moroni, L.M. Galantucci (Eds.), Proc. 5th Int. Conf. Ind. 4.0 Model Adv. Manuf., Springer International Publishing, Cham, 2020: pp. 129–143.

[8] Y. Hua, J. Choi, Feedback control effects on dimensions and defects of H13 tool steel by DMD process, ICALEO 2003 - 22nd Int. Congr. Appl. Laser Electro-Optics, Congr. Proc. 118 (2003). https://doi.org/10.2351/1.5060000.

[9] Q. Wang, J. Li, A.R. Nassar, E.W. Reutzel, W.F. Mitchell, Model-based feedforward control of part height in directed energy deposition, Materials (Basel). 14 (2021) 1–20. https://doi.org/10.3390/ma14020337.

[10] J. Li, Q. Wang, P. Michaleris, E.W. Reutzel, A.R. Nassar, An Extended Lumped-Parameter Model of Melt-Pool Geometry to Predict Part Height for Directed Energy Deposition, J. Manuf. Sci. Eng. Trans. ASME. 139 (2017) 1–14. https://doi.org/10.1115/1.4037235.

[11] F. Caiazzo, A. Caggiano, Laser direct metal deposition of 2024 al alloy: Trace geometry prediction via machine learning, Materials (Basel). 11 (2018). https://doi.org/10.3390/ma11030444.

[12] Y.Y. Woo, S.W. Han, I.Y. Oh, Y.H. Moon, W. Ha, Control of Directed Energy Deposition Process to Obtain Equal-Height Rectangular Corner, Int. J. Precis. Eng. Manuf. 20 (2019) 2129–2139. https://doi.org/10.1007/s12541-019-00226-6.

[13] A. Vandone, S. Baraldo, A. Valente, Multisensor data fusion for additive manufacturing process control, IEEE Robot. Autom. Lett. 3 (2018) 3279–3284. https://doi.org/10.1109/LRA.2018.2851792.

[14] M.T. Dalaee, L. Gloor, C. Leinenbach, K. Wegener, Experimental and numerical study of the influence of induction heating process on build rates Induction Heating-assisted laser Direct Metal Deposition (IH-DMD), Surf. Coatings Technol. 384 (2020) 125275. https://doi.org/10.1016/j.surfcoat.2019.125275.

[15] D.P. Kingma, J.L. Ba, Adam: A method for stochastic optimization, 3rd Int. Conf. Learn. Represent. ICLR 2015 - Conf. Track Proc. (2015) 1–15.